Journal of Materials Chemistry A

PAPER

View Article Online
View Journal | View Issue

Cite this: J. Mater. Chem. A, 2018, 6, 6455

Carbon dioxide capture in the presence of water by an amine-based crosslinked porous polymer†

Mahmoud M. Abdelnaby,[ab] Ahmed M. Alloush,[ac] Naef A. A. Qasem,[c] Bassem A. Al-Maythalony,[c] Rached B. Mansour,[c] Kyle E. Cordova[bd] and Othman Charles S. Al Hamouz*[a]

Received 1st January 2018
Accepted 17th March 2018

DOI: 10.1039/c8ta00012c

rsc.li/materials-a

An amine-functionalized, crosslinked porous polymer is synthesized by linking 1,4-benzenediamine and pyrrole with *p*-formaldehyde in the presence of hydrochloric acid catalyst. The resulting polymer was structurally characterized and proven permanently porous with a surface area of 305 m^2 g^{-1}. The high concentration of amines (–NH– and $–NH_2$) within the backbone of the polymer result in exceptional selectivity (141) for CO_2 over N_2 and dynamic capacity (15.1 cm^3 g^{-1}) in the presence of water (20 : 80 v/v CO_2 : N_2, 91% relative humidity, 1 bar, and 298 K). The performance of this polymer is maintained over 45 cycles without loss of selectivity, capacity, nor recyclability at room temperature; making it stand out among all porous organic materials used for carbon capture.

Introduction

Ever-increasing global CO_2 emissions stemming from the burning of various fossil fuels requires an urgent, yet practical solution.[1] Of the different approaches investigated for solving this challenge, post-combustion CO_2 capture is attractive as one can effectively eliminate the problem at the source.[2] However, current technology relies on expensive, energy inefficient, and corrosive aqueous amine solutions.[3] To implement a more effective post-combustion CO_2 capture process, porous adsorbent materials must be developed.[4] As such, in order to deem a material viable for this application, seven criteria must be considered:[5] (i) relatively high CO_2 adsorption capacity. Since CO_2 represents 15–16% v/v concentration of a flue gas stream, adsorption capacity must be relatively high at low partial pressures (<0.2 bar);[6,7] (ii) high selectivity toward CO_2. Selectivity governs the purity of the CO_2 obtained, which plays a critical role in the economics of the process;[5,7] (iii) fast adsorption kinetics. The adsorption kinetics are sufficiently fast to realize practical implementation. This means that the equilibrium capacity, obtained from thermodynamic isotherms, is similar to the working capacity found in dynamic adsorption;[8] (iv) mild regeneration conditions. The majority of the energy penalty in current post-combustion capture technologies lies in the fact that a substantial energy input is required to regenerate the adsorbent material;[2] (v) long-term stability over the course of extensive use. The material must retain its performance over many adsorption–desorption cycles; (vi) tolerance to other components in a flue gas stream, including and most importantly, water. The majority of conventional porous adsorbent materials (*e.g.* zeolites and porous carbon) suffer from water poisoning.[4] Materials based on reticular chemistry (*i.e.* metal–organic frameworks) have only recently demonstrated their effectiveness in mitigating contaminants, such as water, in flue gas streams;[9–11] and, finally, (vii) low production cost.

Given these criteria, the development of a new porous adsorbent material represents a target worth pursuing. Accordingly, we turned our attention to porous organic polymers, which are viewed as strong candidates to replace current technologies due to their demonstrable high and selective CO_2 uptake in conjunction with their structural diversity and exceptional physicochemical stabilities.[12] A variety of porous organic polymers have been explored[13–19] and several of these materials standout as particularly noteworthy in the context of the aforementioned seven criteria;[20–24] however, there have only been few notable reports, in which such materials were shown to have met most of these criteria.

In this contribution, we report a new porous polymer, termed KFUPM-1, that was synthesized by acid catalyzed polycondensation of the inexpensive (criterion #7), CO_2-philic monomers, pyrrole and 1,4-benzenediamine, with *p*-formaldehyde as the linking agent (Fig. 1). The synthetic design strategy

[a]Department of Chemistry, King Fahd University of Petroleum and Minerals (KFUPM), Dhahran 31261, Saudi Arabia. E-mail: othmanc@kfupm.edu.sa

[b]Center for Research Excellence in Nanotechnology (CENT), KFUPM, Dhahran, 31261, Saudi Arabia

[c]King Abdulaziz City for Science and Technology—Technology Innovation Center on Carbon Capture and Sequestration (KACST-TIC on CCS), KFUPM, Dhahran 31261, Saudi Arabia

[d]Berkeley Global Science Institute, University of California—Berkeley, Berkeley, California 94720, USA

† Electronic supplementary information (ESI) available: Full synthesis and characterization details for KFUPM-1, including FT-IR and NMR spectra, gas adsorption measurements, water adsorption isotherms, and breakthrough experimental details. See DOI: 10.1039/c8ta00012c

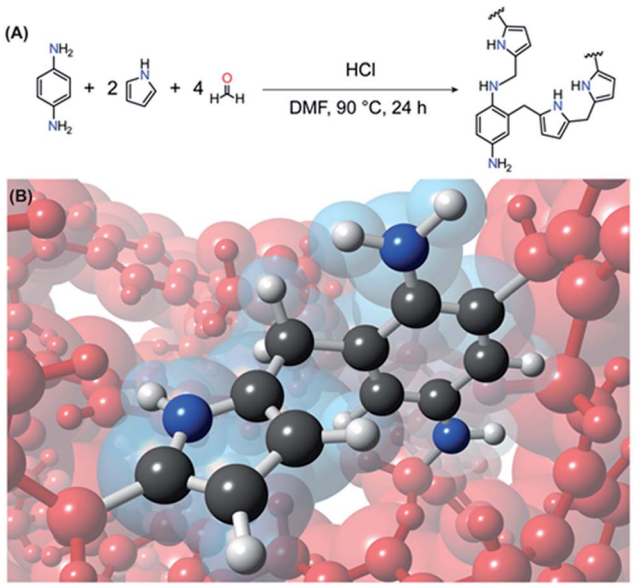

Fig. 1 Important structural features found within the backbone of the crosslinked, porous polymer, KFUPM-1. (A) The synthesis of KFUPM-1 was carried out by linking 1,4-benzenediamine and pyrrole with *p*-formaldehyde in the presence of hydrochloric acid catalyst. (B) The structural features are a pyrrole monomer linked to 1,4-benzenediamine monomer by a methylene unit that is derived from *p*-formaldehyde. Atom colors: C, black; N, blue; and H, white. The surrounding backbone structure of KFUPM-1 is depicted in red.

was founded upon increasing the density of polar aromatic amines within the backbone of the resulting polymer in order to increase the material's affinity to CO_2. KFUPM-1 was proven permanently porous with relatively high CO_2 uptake capacity at relevant partial pressures (criterion #1) and ultrahigh CO_2/N_2 selectivity (criterion #2). Dynamic breakthrough measurements were then performed, in which KFUPM-1 was demonstrated capable of separating CO_2 from both dry and wet (91% relative humidity) gas mixtures – mixtures whose composition mimicked those found in a flue gas stream (criteria #3 and #6). Following this, continuous multicycle breakthrough experiments (>45 cycles) were carried out under wet conditions. These measurements proved that the dynamic CO_2 uptake capacity in the presence of water remained relatively unchanged over 45 cycles (criterion #5). Finally, the ease of regeneration between each cycle was accomplished under mild conditions (criterion #4). When taken together, the findings described herein demonstrate a new material that stands out among all porous organic materials used for carbon capture under practical, industrially relevant conditions.

Experimental section

Materials and methods

Pyrrole (98% purity), 1,4-benzenediamine (98% purity), methanol (99.9% purity), *N*,*N*-dimethylformamide (DMF, 99% purity), and hydrochloric acid (37 wt%) were purchased from Sigma Aldrich Co. Anhydrous iron(III) chloride (≥99.99% purity) was acquired from Alpha Chemika. Paraformaldehyde (≥99% purity) was obtained from Fluka. Ammonium hydroxide (28–30% w/w) was purchased from Fisher Scientific. Pyrrole was distilled under N_2 flow at 418 K and stored under a N_2 environment at 269 K prior to use. All other chemicals were used without further purification. For gas sorption measurements, ultrahigh purity grade nitrogen (99.999%), helium (99.999%), and high purity CO_2 (99.9%) were obtained from Abdullah Hashem Industrial Co., Dammam, Saudi Arabia (see ESI,† Section S1).

Characterization

^{13}C solid state nuclear magnetic resonance (NMR) spectroscopy measurements were performed on a Bruker 400 MHz spectrometer operating at 125.65 MHz (11.74 T) and at ambient temperature (298 K). Samples were packed into 4 mm ZrO_2 rotors and cross-polarization magic angle spinning (CP-MAS) was employed with a pulse delay of 5.0 s and a magic angle spinning rate of 10 kHz for the 1,4-benzenediamine monomer or 14 kHz for the polymer. Fourier transform infrared (FT-IR) spectroscopy measurements were performed from KBr pellets using a PerkinElmer 16 PC spectrometer. The spectra were recorded over 4000–400 cm^{-1} in transmission mode and the output signals were described as follows: s, strong; m, medium; w, weak; and br, broad. Thermal gravimetric analysis (TGA) was run on a TA Q-500 instrument with the sample held in a platinum pan under air flow with a 10 °C per min heating rate. To identify the type of gases trapped within the pores, TGA-mass spectrometry (TGA-MS) analysis was performed using a QMS 403 C Aëolos with STA 449 F1 Jupiter instrument. Powder X-ray diffraction (PXRD) measurements were carried out using a Rigaku MiniFlex II X-ray diffractometer with Cu K_α radiation ($\lambda = 1.54178$ Å). Low pressure nitrogen sorption isotherms were collected on a Micromeritics ASAP 2020. A liquid nitrogen bath was used for the measurements at 77 K. CO_2 sorption isotherms were carried out on an Autosorb iQ2 volumetric gas adsorption analyser. The measurement temperatures at 273 and 298 K were controlled with a water circulator. Water adsorption measurements were performed on a DVS Vacuum, Surface Measurement Systems Ltd, London, UK. Prior to these measurements, KFUPM-1 was pre-treated by heating (383 K) under vacuum for 10 h using the Dynamic Vapor Sorption Analyzer Desorption (Section S1†).

Synthesis of KFUPM-1

For full synthetic details, including optimization experiments, please refer to Section S2.† 1,4-Benzenediamine (1.08 g, 10.0 mmol) and *p*-formaldehyde (1.20 g, 40.0 mmol) were combined in 70 mL DMF in a 100 mL round bottom flask and then stirred at room temperature for 5 min. Pyrrole (1.34 g, 20.0 mmol) was then added and the resulting reaction mixture was stirred for an additional 5 min. After this, 1.6 mL conc. HCl (12 M) was added dropwise into the reaction mixture and the flask was sealed with a rubber septum and purged with N_2 for 2–3 min. The mixture was subsequently heated at 363 K in an oil bath for 24 h with continuous stirring at a rate of 200 rpm. After this time elapsed, a black solid was isolated by filtration. The solid was washed

with 40 mL of methanol followed by sonication for 30 min. The solid was filtered and immersed in an ammonium hydroxide solution (25% w/w) for 24 h, 40 mL distilled water for 24 h, and 60 mL of methanol per d for 3 d with stirring, at which time a clear filtrate solution was obtained. Finally, the product was dried at 348 K under vacuum (<0.1 bar) for 20 h. The final yield (2.56 g) was 88% based on the monomers weights. Elemental Analysis Calcd (%) for $C_{18}H_{20}N_4$: C, 73.94 H, 6.89; N, 19.16. Found C, 52.91; H, 5.03; N, 12.31. FT-IR (KBr, 4000–400 cm^{-1}): 3413 (br), 3240 (br), 2918 (w), 2852 (w), 1618 (m), 1510 (w), 1423 (w), 1024 (w), 671 (m).

Breakthrough measurements

The schematic for the homemade breakthrough system set-up is shown in Section S5.† The bed was packed with KFUPM-1 powder (1.12 g) and the sample was activated at 373 K under vacuum for 24 hours prior to carrying out the breakthrough measurements. The breakthrough experiments were conducted under ambient conditions (298 K and 1 bar) with a 10 sccm flowrate of $CO_2 : N_2$ (20 : 80 v/v) feed mixture. For the measurements under humid conditions, the sample bed was subjected to a stream of wet N_2 gas (91% relative humidity, RH), in which the water level in the gas stream was monitored until saturation was obtained as detected by mass spectrometry. At this point, dry CO_2 was introduced into the wet N_2 stream with the same flowrate as the dry conditions noted above. The full breakthrough capacity of CO_2 was measured by evaluating the ratio of compositions of the downstream gas and the feed gas.

Results and discussion

Synthesis strategy

The underlying objective for this research program was to synthesize a porous polymer based on inexpensive monomers, which contain accessible CO_2-philic functional groups. As such, pyrrole and 1,4-benzenediamine were identified as the monomers since they have integrated polar aromatic amine moieties (known for inducing strong interactions with CO_2) within their molecular structures.[15] The synthetic strategy used to crosslink these CO_2-philic monomers was based on an acid catalyzed polycondensation reaction whereby *p*-formaldehyde would serve as a linking agent. In the quest to optimize the reaction conditions, the solvent (dichloroethane, DMF, or dimethylsulfoxide) and the catalyst (conc. HCl, $FeCl_3$, or CuCl) were varied (Section S2†). Conventional Lewis acid catalyzed polycondensation reactions typically make use of $FeCl_3$ as the catalyst, in equimolar amounts, in order to activate the linking agent;[18] however, our findings demonstrated that the optimized conditions relied on using a catalytic amount of conc. HCl (27 mol% of monomers) with DMF as the solvent. Indeed, these conditions produced the crosslinked, porous polymer product, KFUPM-1, in 88% yield (Fig. 1). It is noted that KFUPM-1 could be synthesized using the other catalysts or solvents, but those products suffered drawbacks resulting from either lower yield, trapped catalyst (Fe) or unreacted species, lower surface area, or lower CO_2 sorption uptake (Section S4†). After synthesis, KFUPM-1 was thoroughly washed with water and methanol followed by a solution of ammonium hydroxide in order to remove any unreacted starting materials and to neutralize any residual acid, respectively. It is noted that in order to prove the complete removal of Cl^- ions, we added $AgNO_3$ to the filtrate, in which no precipitate was found to have formed. Prior to use in further characterization, KFUPM-1 was activated at 348 K under dynamic vacuum for 20 h.

Structural characterization and permanent porosity

Due to the amorphous nature of KFUPM-1, as evidenced by PXRD, the connectivity of the constituents was assessed using a combination of cross polarization-magic angle spinning (CP-MAS) ^{13}C NMR and FT-IR spectroscopies (Section S3†). Accordingly, the ^{13}C NMR spectra of KFUPM-1 revealed two resonances corresponding to CH_2 species: (i) a broad peak centered at $\delta = 24$ ppm, which was assigned to a chemical shift for a CH_2 that links aromatic C atoms from either monomer; and (ii) a lower intensity peak at $\delta = 40$ ppm, which was assigned to a CH_2 linked to the N atom in 1,4-benzenediamine (Fig. 2A). An additional broad resonance, centered at $\delta = 129$ ppm, was assigned to the chemical shifts of aromatic C atoms. The spectral data agree with that in previous reports.[15,16] A shoulder peak at $\delta = 140$ ppm was also noted and attributed to the aromatic C atom to which the amine functionality is located. Further support for these assignments came from observing similar resonances in the ^{13}C NMR spectrum for a model polymer based on the polycondensation of 1,4-benzenediamine with *p*-formaldehyde (Fig. 2B, C) (Section S3†).

To further support the ^{13}C NMR data, FT-IR spectra were collected for the pure pyrrole and 1,4-benzenediamine monomers as well as for KFUPM-1 (Fig. 2D; Tables S3–S6†). The FT-IR spectra for KFUPM-1 exhibited a broad absorption band centered at 3413 cm^{-1}, which is characteristic of the ν_{N-H} stretching frequency. This absorption band is confirmed by the spectrum for the pure pyrrole. Evidence for free amine moieties in KFUPM-1 was provided by the appearance of a shoulder absorption band at ~3240 cm^{-1}, which is also present in the spectrum for the pure 1,4-benzenediamine. The broadening of this band was attributed to trapped water molecules (ν_{O-H} stretching) as evidenced by TGA-MS analysis, which demonstrated that only water molecules were released prior to structural decomposition occurring at 220 °C (Fig. S10†).[25–27] Noteworthy in the FT-IR spectra of KFUPM-1 was the appearance of a new absorption band at 2918 cm^{-1} for methylene ν_{C-H} stretching modes (Fig. 2D). This band was distinctly absent in the spectra for both pure monomers. Finally, the aromatic $\nu_{C=C}$ vibrational mode, situated at 1515 cm^{-1}, for the 1,4-benzenediamine was present in the spectrum of KFUPM-1, which lends strong support for the incorporation of this monomer within the polymer.

The architectural stability and permanent porosity of KFUPM-1 was then investigated by N_2 adsorption isotherm at 77 K (Fig. S12†). At low relative pressures ($P/P_0 < 0.6$), KFUPM-1 exhibited a Type-I profile. At $P/P_0 > 0.6$, a sharp uptake was observed indicating that inter-particle condensation was

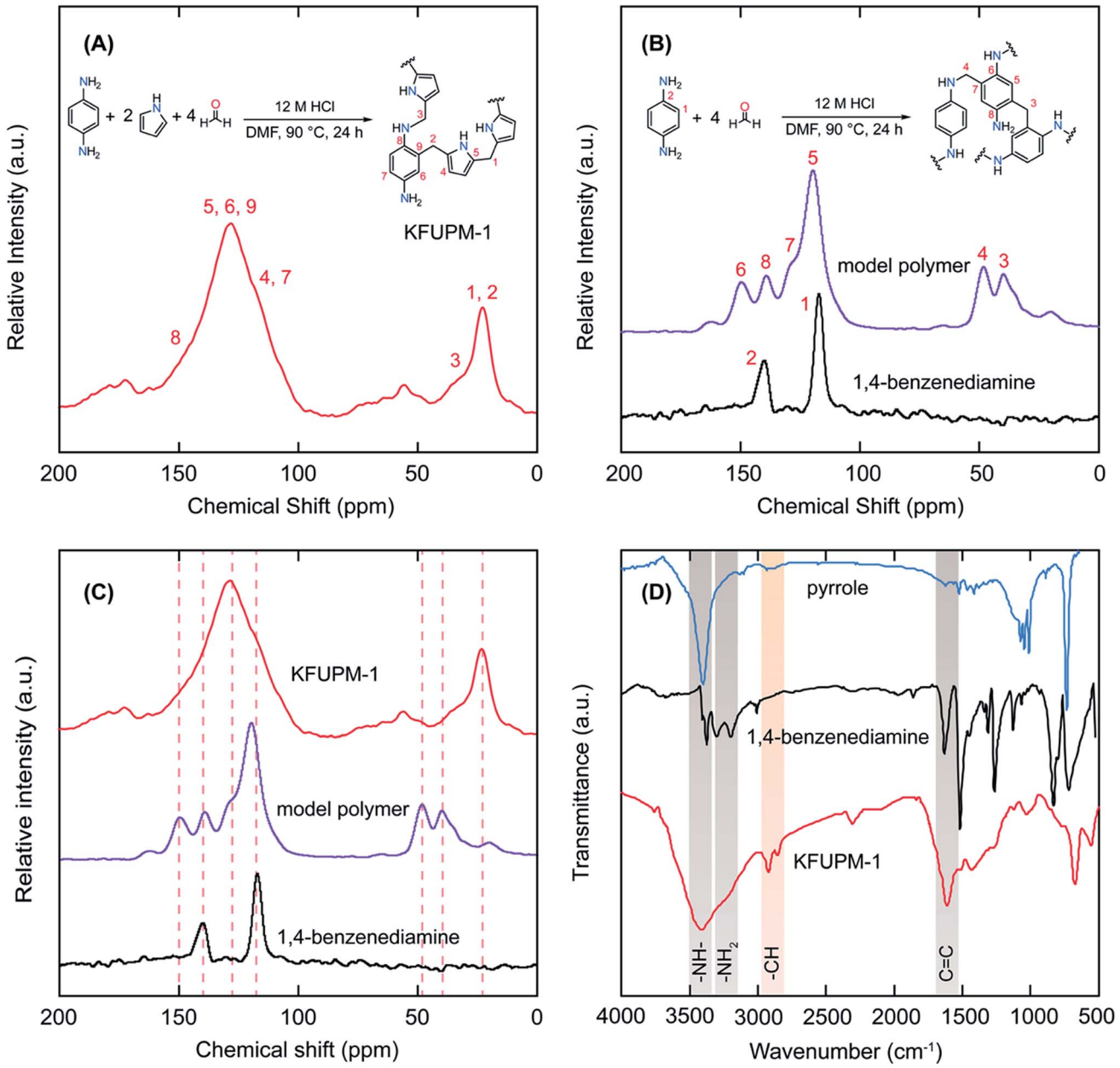

Fig. 2 Structural characterization and solution of KFUPM-1. (A) CP-MAS ^{13}C NMR spectrum of KFUPM-1, with the corresponding core structure of KFUPM-1 provided in the inset for peak assignment. (B) CP-MAS ^{13}C NMR spectra of the model polymer (purple; polycondensation of 1,4-benzenediamine with *p*-formaldehyde) and the 1,4-benzenediamine monomer (black). The corresponding core structure of the model polymer is provided in the inset for peak assignment. (C) Stacked CP-MAS ^{13}C NMR spectra for comparing KFUPM-1 (red), the model polymer (purple), and the 1,4-benzenediamine monomer (black). (D) Fourier transform-infrared spectroscopy (FT-IR) analysis of KFUPM-1 (red) in comparison to pure 1,4-benzenediamine (black) and pure pyrrole (blue). Those absorption bands directly related to the characteristic functionalities of KFUPM-1 are highlighted. The new methylene linkage is highlighted in orange.

occurring (*i.e.* the presence of meso-/macropores between particles). Upon desorption, a small hysteresis was noted likely as a result of elastic deformation or swelling.[28] The Brunauer–Emmett–Teller (BET) model was applied over the $P/P_0 = 0.01$–0.3 range to yield a calculated surface area of 305 $m^2\ g^{-1}$. It is important to note that a relatively uniform pore size distribution indicating that both micro- and mesoporosity was found for KFUPM-1 (Fig. S14†). In terms of practical applicability, the stability of this material toward water was then examined by carrying out water adsorption measurements. Accordingly, the water adsorption isotherm at 298 K for KFUPM-1 displayed a Type-II profile, which indicates that the material is capable of adsorbing 33.5 wt% water at $P/P_0 > 0.9$ (90% RH) (Section S4†). To assess the long-term stability of KFUPM-1 toward water, a multicycle continuous water isotherm at 313 K (>20 cycles) was carried out, which demonstrated that KFUPM-1 was able to retain its water adsorption properties over long periods of time and use (Section S4†).

Gas adsorption properties

Thermodynamic uptake capacity

On the basis of the aromatic amine-rich structure and KFUPM-1's permanent porosity and water stability, we sought to assess the material's thermodynamic gas adsorption properties. Accordingly, low-pressure, single-component gas adsorption isotherms for CO_2 and N_2 were measured at 273 and 298 K up to 760 Torr (Fig. 3). KFUPM-1 exhibits moderate CO_2 uptake capacities of 34.0 $cm^3\ g^{-1}$ at 273 K and 760 Torr and 23.4 $cm^3\ g^{-1}$ at 298 K and 760 Torr. This is in contrast to the N_2 uptake capacities under the same experimental conditions (1.2 and 1.0 $cm^3\ g^{-1}$ at 273 and 298 K, respectively, and 760 Torr). Interestingly, as depicted in Fig. 3, KFUPM-1 displays a much steeper CO_2 uptake in the low-pressure region at 298 K when compared to the N_2 uptake. This observation is indicative of stronger polymer–CO_2 interactions (*i.e.* higher affinity) than is found for N_2, which lends credence to the potential of KFUPM-1 to serve as an adsorbent for selective CO_2 capture from flue gas.

Coverage-dependent enthalpy of adsorption and CO_2/N_2 selectivity

Due to the thermodynamic gas adsorption measurement results, we were encouraged to pursue a deeper understanding of KFUPM-1's relationship with CO_2. Accordingly, the coverage-dependent enthalpy of adsorption (Q_{st}) for CO_2 was estimated by fitting the isotherms collected at 273 and 298 K with a virial-type expansion equation (Section S4†). The resulting initial Q_{st} value was calculated to be 34 kJ mol^{-1}, which quantifiably demonstrates the material's strong binding affinity to CO_2. It is noted that the Q_{st} remained relatively constant, thus, reflecting the homogeneous binding strengths over multiple sites at low coverage. The Q_{st} value is moderately high for physisorption-driven materials as compared to the related materials: BILP-1 (26.5 kJ mol^{-1}),[29] Azo-COP-1 (29.3 kJ mol^{-1}),[30] and PAF-1 (15.6 kJ mol^{-1}).[31] With these results, the CO_2/N_2 selectivity was then estimated based on Henry's law. KFUPM-1 demonstrated a remarkably high CO_2/N_2 selectivity of 249 and 141 at 273 and 298 K, respectively. These values were corroborated by applying Ideal Adsorbed Solution Theory (IAST), which provided information about selectivity with pressure as a consideration (Section S4†). These selectivities are among the highest values reported for crosslinked, porous polymers to date (Table 1).

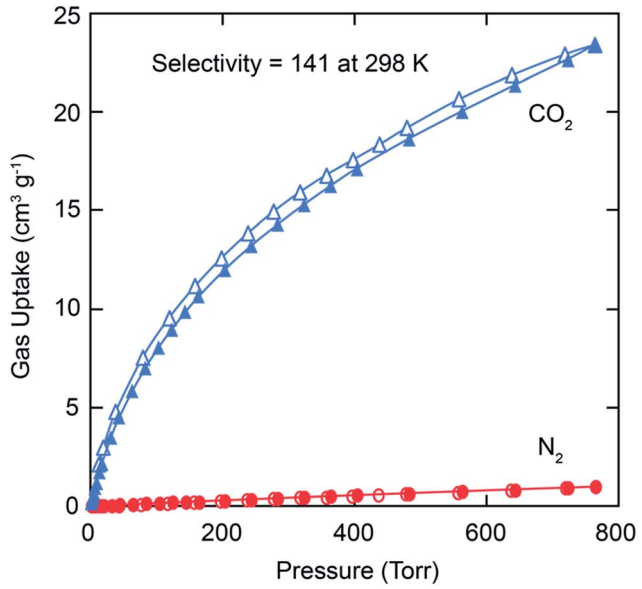

Fig. 3 Gas adsorption properties of KFUPM-1. CO_2 (blue triangle) and N_2 (red circle) adsorption isotherms for KFUPM-1 at 298 K. Filled and open symbols represent adsorption and desorption branches, respectively. The connecting lines serve as a guide to the eye.

Dynamic CO_2 capture by breakthrough experiments

In order to evaluate the performance of KFUPM-1 in effectively and selectively capturing CO_2 under practical flue gas conditions, dynamic breakthrough experiments were implemented. In a typical experiment, an activated sample of KFUPM-1 was loaded into a bed and exposed to a gaseous mixture of 20% (v/v) CO_2 and 80% (v/v) N_2 (volumetric percentages closely resembling flue gas composition) (Section S5†). The effluent was monitored for the breakthrough time (the time in which adsorbed CO_2 'breakthroughs' the bed) by an online mass spectrometer. As seen in Fig. 4, N_2 (red filled triangles) is solely present in the effluent for 4.79 min, at which point the CO_2 (blue filled diamonds) breakthrough point is observed. Clearly, CO_2 is selectively retained by KFUPM-1 for a significant period of time while N_2 passes freely through the material. The corresponding dynamic CO_2 uptake capacity of KFUPM-1, calculated from the breakthrough time, was 8.6 $cm^3\ g^{-1}$. As shown in Table 1, the capacity of KFUPM-1 is comparable to other porous polymers, such as CTF-FUM-350 and CTF-DCN-500 (11.4 and 8.3 $cm^3\ g^{-1}$, respectively),[32] as well as covalent organic frameworks (*e.g.* LZU-301 and $[HO_2C]_{100\%}$–H_2P–COF: 4.9 and 16.4 $cm^3\ g^{-1}$, respectively).[33,34]

Although these results represent initial promise for KFUPM-1, a critical parameter remains untested. In flue gas, water is the third major component by volumetric concentration (5–7%).[6] As such, porous materials typically experience difficulty in selectively capturing CO_2 in the presence of water since competitive adsorption readily occurs.[4] This results in decreased CO_2 uptake capacity and/or a lack of long-term stability and recyclability of the material. Porous materials such as MOFs,[35] zeolitic imidazolate frameworks (ZIFs),[36] and copper silicates[37] have made great strides in capturing CO_2 in the presence of water; however, there remain very few reports of porous polymers that have been investigated for this property.[21–24,26,33] Given KFUPM-1's initial breakthrough results under dry conditions in conjunction with its water stability, we examined the material's ability to separate CO_2 from N_2 in the presence of water. Accordingly, KFUPM-1 was exposed to a ternary gas mixture containing CO_2 (20% v/v), N_2 (80% v/v), and H_2O (91% RH). As shown in Fig. 4, KFUPM-1 was again able to selectively retain CO_2 (blue open diamonds) while N_2 (red open triangles) passed through unencumbered. The longer CO_2 retention time (5.29 min) under wet conditions was not unexpected as KFUPM-1 adsorbs ~33.5 wt% water at 91% RH, which leads to stronger

Table 1 Surface area, CO_2 capture properties, and CO_2/N_2 selectivity for KFUPM-1 in comparison with high performing, similarly related polymeric materials. KFUPM-1 represents one of the highest performing materials among all porous organic materials applied toward the selective capture of CO_2 in the presence of water

Material	A_{BET} ($m^2\ g^{-1}$)	CO_2 uptake[a] ($cm^3\ g^{-1}$)	CO_2/N_2 selectivity[b]	Dynamic CO_2 uptake capacity – wet[c] ($cm^3\ g^{-1}$)	Regeneration temperature (K)	Ref.
KFUPM-1	305	23.4	141	15.1	298	This work
CTF-FUM-350	230	57.2	102	—	—	32
CTF-DCN-500	735	38.4	37	—	—	32
LZU-301	654	35.6	—	8.2	373	33
$[HO_2C]_{100\%}$–H_2P–COF	364	76	77[d]	—	353[e]	34
FCTF-1	662	72	31[d]	14.2	298[f]	22
TB-COP-1	1340	70.7	68[d]	—	—	39
BPL carbon	1210	47	—	4.2	—	36
Azo-COP-1	635	32	96[d]	—	298	30
NUT-6	1138	83.5	338[d]	—	333	40
NUT-10	100[g]	40.2	159[d]	—	333	41
PPN-6-SO_3NH_4	593	81	196	25.8[h]	363	8

[a] At 298 K and 760 Torr. [b] Calculated from single component isotherms by Henry's law. [c] Calculated from dynamic breakthrough experiments. [d] Calculated by ideal adsorbed solution theory at 298 K and 1 bar. [e] Regeneration temperature needed for dry breakthrough experiment. [f] Regenerated under vacuum. [g] Measured by CO_2 adsorption at 273 K. [h] At 313 K. Those properties that were not reported are identified with '—'.

interactions with CO_2. Indeed, this longer retention time has been observed in other systems.[36,38]

The resulting dynamic CO_2 uptake capacity from the ternary gas mixture ($CO_2/N_2/H_2O$) was calculated to be 9.5 $cm^3\ g^{-1}$. For implementation in an industrial setting, an adsorbent material's long-term use and recyclability, without loss in performance, is a critical factor that must be considered. Accordingly, we carried out a multicycle continuous breakthrough measurement (>45 cycles) at 298 K (Fig. 5). For each cycle of this experiment, KFUPM-1 was first exposed to a wet N_2 stream (91% RH) until water saturation was detected. At the point of saturation, a dry stream of CO_2 (20% v/v) was then added to the wet N_2 stream and the effluent was monitored for the breakthrough time. KFUPM-1 exhibited an exceptional stability and recyclability over the course of the multicycle measurements. Although the breakthrough time exhibited non-negligible fluctuation over the course of these cycles, the performance (*i.e.* dynamic CO_2 uptake capacity as measured by breakthrough time) remained relatively unchanged (15 $cm^3\ g^{-1}$) when comparing the 2nd and the 45th cycles (Table 1 and Fig. 5). It is important to

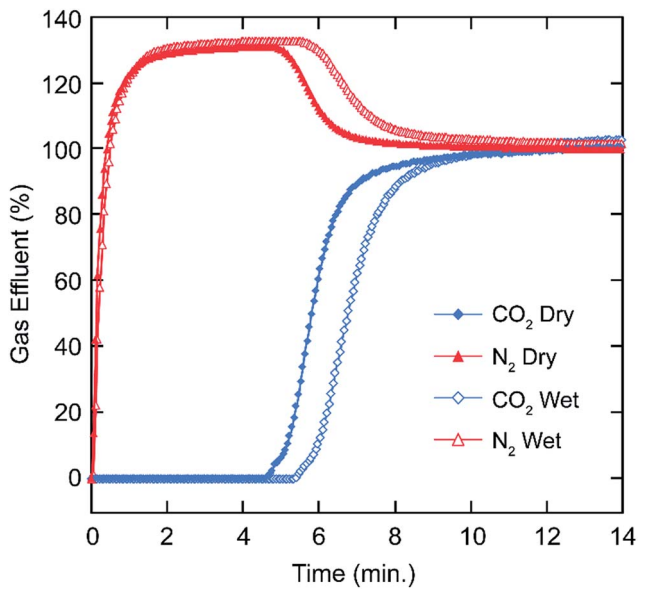

Fig. 4 Dynamic breakthrough measurements demonstrating the ability of KFUPM-1 to separate CO_2 from N_2 under both wet and dry conditions. A 20 : 80 (v/v) gas mixture containing CO_2 and N_2, respectively, under dry (closed symbols) or wet (91% RH, open symbols) conditions was flown through a fixed bed of KFUPM-1 at 298 K and 1 bar.

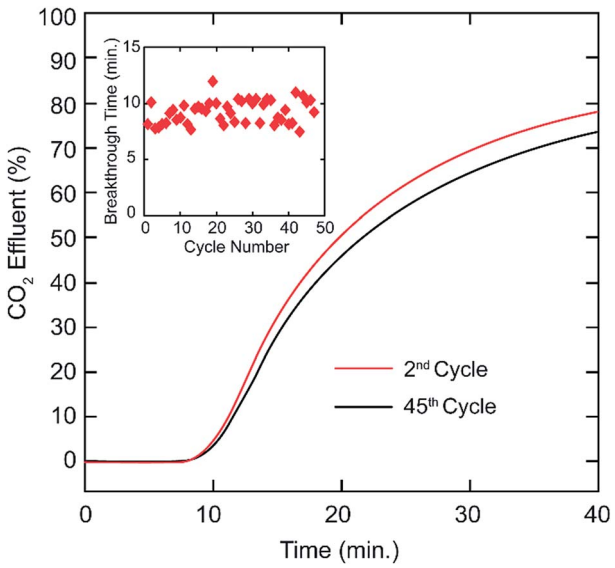

Fig. 5 Long-term recyclability performance of KFUPM-1 as demonstrated by CO_2 breakthrough measurements under wet conditions. There is no loss in dynamic adsorption capacity over 45 consecutive breakthrough measurements. Inset: the breakthrough time as a function of the cycle number.

note that between each cycle, KFUPM-1 was regenerated by simply flowing a wet N_2 stream through the material at 298 K. From an energy cost standpoint, this regeneration procedure represents a remarkably attractive feature for using KFUPM-1 as an adsorbent for the selective capture of CO_2 from real flue gas mixtures.

Conclusion

By developing a new synthetic strategy based on the acid catalyzed polycondensation of pyrrole and 1,4-benzenediamine with *p*-formaldehyde, the novel inexpensive, robust, and CO_2-phillic porous polymer, KFUPM-1, was realized. Taking stock of KFUPM-1's properties and performance in light of the seven criteria needed for developing an effective adsorbent material for post-combustion CO_2 capture, we quickly observe a new material whose performance stands out in an otherwise crowded field for this particular application. Indeed, KFUPM-1 is among the highest performing (or, alternatively, most well-rounded) materials for CO_2 capture under industrially-relevant, practical conditions. With respect to this report, we demonstrated that the connectivity of the constituents comprising KFUPM-1 were successfully determined *via* CP-MAS ^{13}C NMR and FT-IR spectroscopies and the permanent porosity was proven (305 $m^2\ g^{-1}$). The porous material, with its high density of polar, aromatic amines, displayed a moderate CO_2 uptake capacity (23.4 $cm^3\ g^{-1}$) at 298 K along with a moderately high coverage-dependent enthalpy of adsorption ($Q_{st} = 34$ kJ mol^{-1}). When comparing the CO_2 uptake with that of N_2, a CO_2/N_2 selectivity of 249 at 273 K and 141 at 298 K was calculated. These selectivity values are among the highest reported for a porous polymer. With these results in hand, KFUPM-1 was explored for its ability to selectively capture CO_2 from a binary (CO_2/N_2) and ternary ($CO_2/N_2/H_2O$) gas mixture *via* breakthrough measurements. Accordingly, KFUPM-1 demonstrated dynamic CO_2 uptake capacities under dry and wet conditions of 8.6 and 15.1 $cm^3\ g^{-1}$, respectively. Furthermore, a multicycle continuous breakthrough measurement (45 cycles), whereby the regeneration of KFUPM-1 between each cycle was energy efficient, demonstrated that our material was able to selectively capture CO_2 from a wet N_2 stream over long periods of time without significant loss in performance. The findings reported herein highlight a strategy for progressing porous polymers as potential and rationale adsorbent materials for industrially-relevant, practical gas separation processes.

Conflicts of interest

There are no conflicts to declare.

Acknowledgements

We acknowledge Prof. Zain H. Yamani (CENT, KFUPM) for use of CENT facilities and Mr Tom M. Osborn Popp (UC Berkeley) for valuable discussions related to solid state NMR. This work was supported by KFUPM (Project No. IN161034) as well as by the Saudi Aramco Carbon Capture and Utilization Chair Program (Project No. ORCP2390). B. A. A. M. acknowledges support from KACST-TIC on CCS for adsorption measurements. Finally, we are grateful to Prof. Omar M. Yaghi (UC Berkeley) for his support of global science initiatives.

References

1 M. R. Raupach, G. Marland, P. Ciais, C. Le Quéré, J. G. Canadell, G. Klepper and C. B. Field, *Proc. Natl. Acad. Sci. U. S. A.*, 2007, **104**, 10288–10293.
2 R. S. Haszeldine, *Science*, 2009, **325**, 1647–1652.
3 G. T. Rochelle, *Science*, 2009, **325**, 1652–1654.
4 (*a*) S. Choi, J. H. Drese and C. W. Jones, *ChemSusChem*, 2009, **2**, 796–854; (*b*) J. Wang, L. Huang, R. Yang, Z. Zhang, J. Wu, Y. Gao, Q. Wang, D. O'Hare and Z. Zhong, *Energy Environ. Sci.*, 2014, **7**, 3478–3518.
5 A. Sayari, Y. Belmabkhout and R. Serna-Guerrero, *Chem. Eng. J.*, 2011, **171**, 760–774.
6 E. J. Granite and H. W. Pennline, *Ind. Eng. Chem. Res.*, 2002, **41**, 5470–5476.
7 M. T. Ho, G. W. Allinson and D. E. Wiley, *Ind. Eng. Chem. Res.*, 2008, **47**, 4883–4890.
8 W. Lu, W. M. Verdegaal, J. Yu, P. B. Balbuena, H.-K. Jeong and H.-C. Zhou, *Energy Environ. Sci.*, 2013, **6**, 3559–3564.
9 C. A. Trickett, A. Helal, B. A. Al-Maythalony, Z. H. Yamani, K. E. Cordova and O. M. Yaghi, *Nat. Rev. Mater.*, 2017, **2**, 17045.
10 N. T. T. Nguyen, H. Furukawa, F. Gándara, H. T. Nguyen, K. E. Cordova and O. M. Yaghi, *Angew. Chem., Int. Ed.*, 2014, **53**, 10645–10648.
11 P. J. Milner, R. L. Siegelman, A. C. Forse, M. I. Gonzalez, T. Runčevski, J. D. Martell, J. A. Reimer and J. R. Long, *J. Am. Chem. Soc.*, 2017, **139**, 13541–13553.
12 L. Zou, Y. Sun, S. Che, X. Yang, X. Wang, M. Bosch, Q. Wang, H. Li, M. Smith, S. Yuan, Z. Perry and H.-C. Zhou, *Adv. Mater.*, 2017, 1700229.
13 R. Dawson, E. Stöckel, J. R. Holst, D. J. Adams and A. I. Cooper, *Energy Environ. Sci.*, 2011, **4**, 4239.
14 H. Gao, L. Ding, W. Li, G. Ma, H. Bai and L. Li, *ACS Macro Lett.*, 2016, **5**, 377–381.
15 Y. Luo, B. Li, W. Wang, K. Wu and B. Tan, *Adv. Mater.*, 2012, **24**, 5703–5707.
16 S. Dey, A. Bhunia, D. Esquivel, C. Janiak, M. Mastalerz, H. Xia, Y. Mu, X. Xiong, C. Pan, S. Li, S. Qiu and G. Zhu, *J. Mater. Chem. A*, 2016, **4**, 6259–6263.
17 S. Hug, L. Stegbauer, H. Oh, M. Hirscher and B. V. Lotsch, *Chem. Mater.*, 2015, **27**, 8001–8010.
18 L. Tan, B. Tan, T. Fei, T. Zhang, S. Ghasimi, H. Lu, K. Landfester, K. A. I. Zhang, H. Liu, G. Ouyang, J. Hu, H. Liu, S. Dai, C. E. Snape, T. C. Drage, A. I. Cooper, A. Steiner and A. I. Cooper, *Chem. Soc. Rev.*, 2017, **203**, 752–758.
19 M. Seo, S. Kim, J. Oh, S.-J. Kim and M. A. Hillmyer, *J. Am. Chem. Soc.*, 2015, **137**, 600–603.
20 L.-B. Sun, A.-G. Li, X.-D. Liu, X.-Q. Liu, D. Feng, W. Lu, D. Yuan and H.-C. Zhou, *J. Mater. Chem. A*, 2015, **3**, 3252–3256.

21 R. T. Woodward, L. A. Stevens, R. Dawson, M. Vijayaraghavan, T. Hasell, I. P. Silverwood, A. V. Ewing, T. Ratvijitvech, J. D. Exley, S. Y. Chong, F. Blanc, D. J. Adams, S. G. Kazarian, C. E. Snape, T. C. Drage and A. I. Cooper, *J. Am. Chem. Soc.*, 2014, **136**, 9028–9035.
22 Y. Zhao, K. X. Yao, B. Teng, T. Zhang and Y. Han, *Energy Environ. Sci.*, 2013, **6**, 3684–3692.
23 R. Dawson, L. A. Stevens, T. C. Drage, C. E. Snape, M. W. Smith, D. J. Adams and A. I. Cooper, *J. Am. Chem. Soc.*, 2012, **134**, 10741–10744.
24 G.-P. Hao, W.-C. Li, D. Qian, G.-H. Wang, W.-P. Zhang, T. Zhang, A.-Q. Wang, F. Schüth, H.-J. Bongard and A.-H. Lu, *J. Am. Chem. Soc.*, 2011, **133**, 11378–11388.
25 G. Liu, Y. Wang, C. Shen, Z. Ju, D. Yuan, C. T. Yavuz, A. Coskun, E. W. Hagaman, Z. Bian, J. H. Zhou, J. Hu, H. Liu and S. Dai, *J. Mater. Chem. A*, 2015, **3**, 3051–3058.
26 J. Han, Z. Du, W. Zou, H. Li and C. Zhang, *Ind. Eng. Chem. Res.*, 2015, **54**, 7623–7631.
27 P. Puthiaraj and W.-S. Ahn, *Ind. Eng. Chem. Res.*, 2016, **55**, 7917–7923.
28 J. Weber, M. Antonietti and A. Thomas, *Macromolecules*, 2008, **41**, 2880–2885.
29 M. G. Rabbani and H. M. El-Kaderi, *Chem. Mater.*, 2012, **24**, 1511–1517.
30 H. A. Patel, S. H. Je, J. Park, D. P. Chen, Y. Jung, C. T. Yavuz and A. Coskun, *Nat. Commun.*, 2013, **4**, 1357.
31 W. Lu, J. P. Sculley, D. Yuan, R. Krishna, Z. Wei and H.-C. Zhou, *Angew. Chem., Int. Ed.*, 2012, **51**, 7480–7484.
32 K. Wang, H. Huang, D. Liu, C. Wang, J. Li and C. Zhong, *Environ. Sci. Technol.*, 2016, **50**, 4869–4876.
33 Y.-X. Ma, Z.-J. Li, L. Wei, S.-Y. Ding, Y.-B. Zhang and W. Wang, *J. Am. Chem. Soc.*, 2017, **139**, 4995–4998.
34 N. Huang, X. Chen, R. Krishna and D. Jiang, *Angew. Chem., Int. Ed.*, 2015, **54**, 2986–2990.
35 K. E. Cordova and O. M. Yaghi, *Mater. Chem. Front.*, 2017, **1**, 1304–1309.
36 N. T. T. Nguyen, T. N. H. Lo, J. Kim, H. T. D. Nguyen, T. B. Le, K. E. Cordova and H. Furukawa, *Inorg. Chem.*, 2016, **55**, 6201–6207.
37 S. J. Datta, C. Khumnoon, Z. H. Lee, W. K. Moon, S. Docao, T. H. Nguyen, I. C. Hwang, D. Moon, P. Oleynikov, O. Terasaki and K. B. Yoon, *Science*, 2015, **350**, 302–306.
38 A. O. Yazaydın, A. I. Benin, S. A. Faheem, P. Jakubczak, J. J. Low, R. R. Willis and R. Q. Snurr, *Chem. Mater.*, 2009, **21**, 1425–1430.
39 J. Byun, S.-H. Je, H. A. Patel, A. Coskun and C. T. Yavuz, *J. Mater. Chem. A*, 2014, **2**, 12507.
40 S. Mane, Z. Y. Gao, Y. X. Li, D. M. Xue, X. Q. Liu and L. B. Sun, *J. Mater. Chem. A*, 2017, **5**, 23310–23318.
41 S. Mane, Z. Y. Gao, Y. X. Li, X. Q. Liu and L. B. Sun, *Ind. Eng. Chem. Res.*, 2018, **57**, 250–258.

